INSTITUTE FOR FUSION STUDIES

DOE/ET-53088-515 IFSR #515

Effects of a Stratified Atmosphere on the Production of X-Ray and Particle Energy Spectra in Solar Flares

KATHERINE HOLCOMB
Computation Ctr., UT-Austin, Texas 78712 and
NCAR, Boulder, CO 80307

TOSHI TAJIMA
IFS, UT-Austin, Texas 78712

BARUCH MEERSON
Ctr. for Plasma Physics, Racah Inst. of Physics
Hebrew University, Jerusalem, Israel

August 1991

THE UNIVERSITY OF TEXAS

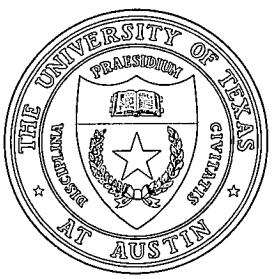

AUSTIN

Effects of a Stratified Atmosphere on the Production of X-Ray and Particle Energy Spectra in Solar Flares

Katherine Holcomb
Computation Center, University of Texas at Austin, Austin, Texas
and
National Center for Atmospheric Research, Boulder, Colorado*

Toshiki Tajima
Institute for Fusion Studies and Department of Physics,
University of Texas at Austin, Austin, Texas
and

Baruch Meerson
Center for Plasma Physics, Racah Institute of Physics,
Hebrew University, Jerusalem, Israel

ABSTRACT

In a stratified solar corona in which the Alfvén speed increases with height, compressional Alfvén waves can accelerate particles to high energies by the mechanism of phase-locked trapping. We demonstrate by numerical simulations that this mechanism can produce power-law spectra of electron and photon energy, both of which show strong similarities, in quantities such as the exponent indices, to the spectra actually observed in X-ray flares and solar energetic particle (SEP) events. Isotopic effects of ^{4}He and ^{3}He ions are also studied in order to explore a possible mechanism for heavy-ion enrichment of such flares.

I. Introduction

Impulsive solar flares can accelerate particles to very high energies, up to 10–100 keV for electrons, and occasionally up to several GeV for ions. Many authors have investigated the mechanism of impulsive flares (Spicer *et al.* 1986, Tajima *et al.* 1987). Most of these flare models are based on magnetohydrodynamic phenomena, and some of the more successful ones are able to discuss the overall energetics, such as the origin of the flare energy, as well as the storage and release mechanisms, and so forth. However, these theories rarely predict the specifics, such as the photon and particle energy spectra. This is partially true because these models do not allow the kinetic processes which are necessary to explore particle acceleration in, or during, flares. On the other hand, much work has been devoted to the acceleration processes *per se* which could account for high-energy spectra of photons and particles during a flare, given the accompanying shocks, reconnection, waves, etc. The most commonly-accepted mechanism for this particle acceleration is first-order Fermi acceleration, in which particles are accelerated by hydromagnetic shocks (Zirin 1988). In certain circumstances, second-order Fermi acceleration (or stochastic acceleration) could operate, but this mechanism is probably too slow for impulsive flares (Nakajima *et al.* 1983; Forrest and Chupp 1983; Kane *et al.* 1986; Forman, Ramaty, and Zweibel 1986). However, even in these models, quantitative energy spectra are seldom predicted, except for the Bessel-function distribution obtained from stochastic heating. To our best knowledge, the effects of atmospheric stratification on the flare energy spectra have never been accomodated in a quantitative theoretical framework. In the present paper, we investigate the effect of the stratified solar atmosphere (more precisely, the corona) on the production of X-ray and charged-particle energy spectra from flares. In previous work (Tajima *et al.* 1987), it was found that

impulsive flares could accompany strong shocks, or more specifically, compressional Alfvén waves, upon the sudden reconnection or realignment of magnetic fields. Therefore, in our current investigation, we consider the acceleration of particles by strong compressional Alfvén waves in a stratified plasma.

We describe here a model for a means by which magnetic energy could be converted into particle energy. It may operate entirely on its own, or it may provide an initial acceleration for particles which are then further accelerated by the first-order Fermi mechanism. Consider first a uniform atmosphere. Particles moving at velocities within the "trapping width" $v_{\rm trap} \sim \sqrt{qE/mk}$ of the phase velocity of an Alfvén wave are accelerated by phase-locking. Acceleration occurs roughly linearly in time in this case (Sakai and Ohsawa 1987), and in a short while, the particle exits from the trapping and ceases to be accelerated. Now consider an atmosphere in which the Alfvén speed *increases* with increasing height. As the particles are accelerated, the phase velocity of the wave increases along with the velocity of the particles, thus leading to acceleration for an extended interval of time. Ultimately, of course, the acceleration must end, but in a non-uniform atmosphere, considerable acceleration can build up before the particles are detrapped. This should be a realistic scenario for the solar corona, where we assume the particles are accelerated.

Impulsive solar flares are often accompanied by large enrichments in heavy ions, particularly ^{3}He and iron. The enrichment of ^{3}He can be particularly striking, with ratios of ^{3}He/^{4}He of order unity, compared to typical solar values for this ratio of approximately 10^{-4}. Recent observations (Lin 1987 and references therein) have indicated that virtually all ^{3}He-enriched events are associated with electron impulsive events.

II. Theory

It has been shown that in the case of a wave with a non-uniform phase velocity, detrapping can be delayed considerably, and particles can be accelerated to high energies, if the phase velocity increases appropriately as the acceleration proceeds (Meerson 1990). In the atmosphere of the Sun, the phase velocity of Alfvén waves should increase with increasing altitude, since the density ought to decrease rapidly; thus we expect that the continuous-acceleration mechanism can operate in such an atmosphere.

A simple analysis will demonstrate the phenomenon. Assume that the background field, B_0, is along the z axis, and suppose that there is a sinusoidal (i.e. wave) longitudinal electric field, of amplitude E, in the x-direction. For simplicity, in the present analysis we will vary B_0, rather than the density. The relativistic equations of motion are then:

$$\frac{dp_x}{dt} = \frac{q}{c} v_y B_0 - qE \sin(kx - \omega t) \ , \tag{2.1}$$

$$\frac{dp_y}{dt} = -\frac{q}{c} v_y B_0 \ , \tag{2.2}$$

where $\vec{p} = m\Gamma\vec{v}$, and Γ is the special-relativistic boost factor. Assume that initially the particle is moving only along the x-direction. The trapping occurs for particles whose velocity matches the phase velocity of the wave, that is, $v_x = \omega/k$. (Thus an increasing Alfvén velocity will lead to acceleration of the trapped particles.) Substituting into (2.2) yields the equation for magnetic trapping at the phase velocity of the wave:

$$\frac{dp_y}{dt} = -\frac{q}{c}\frac{\omega}{k} B_0(x) \ . \tag{2.3}$$

Using $x = \omega t/k$ to integrate the equation of motion (2.3), and ignoring small initial thermal velocities, we find that there will be *continuous acceleration*, provided that

$$B_0(x) \int_0^x B_0(x')dx' < \frac{mc^2 E}{|q|} , \tag{2.4}$$

that is, trapping is maintained as long as the magnetic term in equation (2.1) is small relative to the electric term. Ultimately, the trapping condition may be broken, due to a weakening wave amplitude and/or to a B_0 which does not decrease sufficiently rapidly, and the acceleration will cease. (Excessively prompt decrease of B_0 is not permitted, however, or the adiabatic condition for the acceleration can be violated.) In the meantime, however, the trapped particles can be driven to relativistic velocities.

We can write the equations of motion, (2.1) and (2.2), in dimensionless form by defining $X = kx$, $T = \omega t$, $P_i = kp_i/m\omega$, and $\varepsilon = qEk/m\omega^2$, where k is the wavenumber. The equations then take the form

$$\frac{dP_x}{dT} = \varpi \frac{P_y}{\Gamma} - \varepsilon \sin(X - T) , \qquad \frac{dp_y}{dt} = -\varpi \frac{P_x}{\Gamma} , \tag{2.5}$$

with $dX/dT = P_x/\Gamma$ to complete the set. We have defined $\varpi \equiv \omega_c/\omega$, where ω_c is the cyclotron frequency $\omega_c = qB_0/mc$. These equations are characterized by only two parameters, ε and ϖ, and can easily be solved numerically to investigate the behavior for arbitrary values of those parameters. In order to demonstrate the effect of the phased-locked trapping for a spatially-increasing Alfvén velocity, we parametrize ϖ as, for example,

$$\varpi = \frac{\varpi_0}{1 + \alpha X} , \tag{2.6}$$

where α^{-1} is the scale height, in units of k^{-1}.

Figure 1 shows the results of the solution of equations (2.5) for the parameter values $\varepsilon = 0.5$, $\varpi_0 = 0.035$, and with initial conditions $P_x = 0$, $P_y = 0.2$. For simplicity, we have assumed that the dispersion relation of the wave is $\omega = v_A k$. In Figure 1(a) we show the result for a uniform magnetic field, $\alpha = 0$, while in Figure 1(b), $\alpha = 0.01$. In the uniform case, detrapping occurs quickly, and the particle begins to execute Larmor oscillations. Relativistic effects change the exact form of the solution somewhat, but they do not prevent the detrapping. The stratified atmosphere, on the other hand, can greatly inhibit the detrapping and enhance the acceleration time (and thus the energy), as a comparison of Figures 1(a) and 1(b) shows.

III. Simulations and Results

We carried out computer simulations of the propagation of a compressional Alfvén wave in a stratified solar corona by employing a $1\frac{2}{2}$-dimensional particle-mesh code, for which all three components of momentum are computed, but all quantities are functions of only one space dimension. The density of our model atmosphere (in this case, corona) decreased exponentially, with a scale height of approximately 20decrease in density was accomodated in the code by weighting each particle appropriately to its initial position on the grid (see e.g. Tajima 1989). SEP's are believed to be accelerated in the corona (Fan *et al.* 1984), so our atmosphere setup is intended as a crude model of an isothermal atmosphere. However, the most important phenomenon for this mechanism is the increase in Alfvén speed with increasing height. We constructed a very simple model for our simulation. The parameters we chose are somewhat arbitrary, but they have been varied, with qualitatively similar results. Moreover, computational

convenience requires "compressed" parameters, such as the mass ratio of electrons to ions. It is noted, for example, that when the dynamical time scales are of Alfvén and acoustic origin, the ratio of electron cyclotron period to ion cyclotron period has little effect on the physics involved. In the particular atmospheric run shown here, we initialized a plasma with $\beta \sim 0.04$, $c_s/c \sim 0.055$, and $v_A/c \sim 0.4$. Reflecting boundary conditions ("Method II" of Naitou *et al.* 1979) were employed; this made sure that particles did not leave the grid at one end and reenter with an inappropriate weight at the other end. Because flares are transient events, the Alfvén wave was set up as a pulse, rather than as a wave train. The electric field of the Alfvén wave was initialized such that $E_y/B_0 = 0.2$. The wave packet consisted of a wave train in an exponential envelope with an e-folding of 50 zones; the packet initially occupied the region between approximately zones 150 and 350. There were a total of 19200 electrons, 11520 protons, and 3840 ^{4}He ions in 2048 grid zones. Figure 2 shows the initial density distribution for the electrons. For the run whose results we show here, the ratio q/m of electron mass to ion mass was 1/100 for protons, 2/400 for ^{4}He, and 2/300 for ^{3}He; another run with the ratio of electron to proton mass set to 1/10 gave qualitatively similar results.

In addition to the particles specified above, whose motions were computed self-consistently with the electric and magnetic field, we included 1000 test particles, representing ^{3}He, which responded to the fields but did not contribute to them. This leads to an ^{3}He/^{4}He ratio much higher than the typical photospheric value, but even so, the test particles are minimally resolved. Thus we could not predict a value for this ratio, but can only determine whether ^{3}He might be overheated relative to ^{4}He.

We assumed that particle energy was converted to photons by electron bremsstrahlung. We used the formula

$$g(\varepsilon) = N_0 \frac{mc^2}{\varepsilon} \int_\varepsilon^\infty \frac{1}{(1 + E_k/mc^2)^3} f(E_k)\, dE_k \ , \tag{3.1}$$

where E_k is the kinetic energy of the electrons, and $f(E_k)$ is the kinetic-energy distribution of the electrons obtained from our simulations. It is approximately valid for both nonrelativistic and relativistic regimes, as long as the particles are not ultrarelativistic. The constant N_0 was chosen as a normalization factor.

Observations of X-ray flares show several characteristic features. The energy spectra of both charged particles and photons show signatures of strongly-accelerated particles, and are generally characterized by a power-law shape, rather than a thermal shape. The photon spectrum is generally well-fit by a double power law, with a break energy which varies with the flare and with time, but is generally approximately 100 keV, with power-law exponents below the break energy roughly in the range -2.5 to -3.5 and above the break energy of approximately -3.5 to -6 (Lin and Schwartz 1987). The electron energy spectrum is typically a double or triple power law, with the first break energy at approximately 100 keV for several different flares, and power-law exponents of approximately -0.6 to -2.0 for the first power law, -2.4 to -4.3 for the second, and -3.6 for the third, when it is present (Lin *et al.* 1982). Electron energy spectra extend from approximately 10^3 keV to 10^4 keV, depending on the flare (Lin *et al.* 1982).

In Figures 3–14, we show our results. Figure 3 is the photon spectrum, obtained from Eq. (3.1) above. The spectrum can be fitted by a double power law, with an exponent of -3.3 from approximately 60 to 300 keV, and -6.2

from 300 keV to 1000 keV. The predicted break energy, 300 keV, is higher than the break energy of approximately 100 keV observed in the flare described by Lin and Schwartz (1982) of 1980 June 27; however, the exponents are very comparable to those observed early in that particular X-ray burst.

Figure 4 shows the computed electron energy distribution function at $t = 800\omega_{pe}$. This energy spectrum can be fitted by a double power law; the first from approximately 20 keV to 90 keV, with an exponent of approximately -1.3, and the second from 90 keV to 650 keV, with an exponent of approximately -2.1. The data for electron energy continues to above 1000 keV, but rapidly becomes noisy beyond about 700 keV. The exponent of the first power law is very comparable to that observed in several X-ray flares (Lin *et al.* 1982), while the break energy is very close to that observed. The exponent of the second power law is somewhat less steep than is typically observed for flares with electron energy cutoffs near 1000 keV, although it is comparable to some values observed between $\sim$ 100 keV and $\sim$ 1000 keV for more energetic flares, whose electron energy ranges up to 10^4 keV. Figure 5 is a phase-space plot for the electrons of normalized (to mc) longitudinal momentum versus grid position. The heating of the electrons near the origin is evident, and is due to the slow magnetosonic wave.

In Figure 6, we display the energy distribution function for protons, again at $t = 800\omega_{pe}$. The spectrum can again be represented by a double power law, with an exponent of approximately -1.2 between 200 and 2000 keV, and approximately -2.6 from 2000 to 10^4 keV. The values of the exponents we obtain are less than those observed for protons by Gloeckler (1984), but the shape (a double power law) is consistent, and the knee at approximately 2 MeV is

consistent with the observed break energy, which can be roughly 1 MeV. Figure 7 shows the normalized phase-space plot for protons. In this case, both heating by the slow magnetosonic wave, and acceleration by the fast magnetosonic wave, is evident.

Figure 8 shows the energy distribution function for ^{4}He. This distribution function is quite interesting, because it is extremely non-thermal from 1 MeV to 10 MeV. The accumulation of particles in the high-energy tail is attributed to particularly efficient phase-locking acceleration. Figure 9 is the phase-space plot for ^{4}He. The acceleration at the fast magnetosonic wave is pronounced in this case, and very little heating *per se* occurs. Figure 10 shows the normalized transverse momentum versus the normalized longitudinal momentum for ^{4}He. It is clear that there is substantial preferential longitudinal acceleration in this case.

Figures 11 through 13 show the same quantities for ^{3}He. The deviation from a thermal distribution is particularly striking in this case, as can be seen in Figure 11. However, ^{3}He is accelerated comparably to ^{4}He overall in our numerical experiments.

Figure 14 is a plot of the z-component of the magnetic field, again at time $t = 800\omega_{pe}$. The leading edge of the fast magnetosonic wave is at a grid position of approximately $x = 820$, a location which corresponds to the "spikes" in the accelerated ions (protons as well as helium ions).

IV. Discussion

We have used a simple model of Alfvén-wave acceleration in a stratified atmosphere to model the acceleration of particles in a solar X-ray flare by the mechanism of phase locking. Our model assumes that the process occurs very close to the solar surface, i.e. we cannot model a large-scale region of the corona, and we do not include the effects of bulk mass motion. Further processing of the particles could occur in the solar wind. Nevertheless, we find a quantitative agreement between our computational results and observed quantities, even though we made no special attempt to fit the observed spectra. The resemblance between the computational results and the observations is particularly good for the electron energy spectrum. In many flares, the electron energy is a significant fraction of the total flare energy (Lin *et al.* 1982); thus a mechanism such as that described here, which provides for a direct conversion of magnetic energy into electron energy, is particularly attractive.

Shock heating has been invoked to explain impulsive flares and SEP's (Sakai and Ohsawa, and references therein), but previous work did not include the effects of stratification, and power-law spectra were not produced. The stochastic acceleration model has been reasonably successful at predicting the general shape of the energy spectra (Forman *et al.* 1986); however, it operates on relatively long timescales. The production of the power-law energy spectra, instead of the exponential or Gaussian energy spectra, may be attributable to the mechanism of populating successively higher energy particles. A general discussion along these lines may be found in Mima *et al.* (1991). Our mechanism not only resembles the data (although we have made no quantitative fits), but also naturally provides a *prompt* acceleration mechanism.

Gamma-ray flares are associated with very high-energy protons (Chupp 1984). Such flares may have a different origin, or an additional mechanism, such as a flow driven by violent motion close to the Alfvén speed (e.g. violent reconnection).

The mechanism produces hot ^{4}He (see Fan *et al.* 1984) but is less successful at explaining observations of heavy ions simultaneously. It does produce considerable non-thermal acceleration of ^{4}He and ^{3}He in our simulation, but since those accelerations are comparable, it does not account for the great enhancement in ^{3}He that is observed in some of the SEP events. However, it could provide a partial answer to this mystery, by generating one stage of acceleration of heavy ion species which contributes to the operation of some other, as yet unexplained, mechanism.

Some caveats should be mentioned with regard to our simulations. The usual limitations of a particle-in-cell code apply here; parameters must be "compressed," in some sense, in order to maintain computational feasibility (Tajima 1989). In particular, the mass ratio of protons to electrons is a factor of 100 in our simulations, which can affect the precise appearance of our results, especially the exponents of the power laws. However, the generic physical behavior is not dependent on code parameters such as the mass ratio. Within these limitations, our simple model is quite successful at explaining observations of energy spectra for impulsive X-ray flares.

References

Chupp, E.L. 1984 Ann. Rev. Astr. Ap. **22**, 359.

Fan, C.Y., Gloeckler, G., and Hovestadt, D. 1984 *Space Science Reviews* **38**, 143.

Forman, M. A., Ramaty, R., and Zweibel, E. G., 1986 in "Physics of the Sun," Volume II, ed. P. Sturrock *et al.* (D. Reidel), pp. 49-289.

Forrest, D.J. and Chupp, E.L. 1983 Nature **305**, 291.

Gloeckler, G. 1984 *Adv. Space Res.* **4**, 127 1984.

Kane, S.R., Chupp, E.L., Forrest, D.J., Share, G.H., and Rieger, E. 1986 Ap. J. **300**, L95.

Lin, R. P., Mewaldt, R. A., and Van Hollebeke, M. A. I. 1982 *Ap. J.* **253**, 949.

Lin, R. P. 1987 *Reviews of Geophysics* **25**, 676.

Lin, R. P., and Schwartz, R. A. 1987 *Ap. J.* **312**, 462.

Meerson, B. 1990 Phys. Lett. **A150**, 290.

Mima, K., Horton, W., Tajima, T., and Hasegawa, A. 1991 in "Nonlinear Dynamics and Particle Acceleration" eds. Y.H. Ichikawa and T. Tajima (AIP, New York) p. 27.

Naitou, H., Tokuda, S., Kamimura, T. 1979 J. Comp. Phys. **33**, 86.

Nakajima, H., Kosugi, T., Kai, K., and Ecome, S. 1983 Nature **305**, 292.

Sakai, J.-I., and Ohsawa, Y. 1987 *Space Science Reviews* **46**, 113.

Spicer, D.S., Mariska, J.T., and Boris, J.P. 1986 in "Physics of the Sun" II ed. P. Sturrock *et al.* (Reidel, Nordrecht).

Tajima T. *et al.* 1987 Ap. J. **321**, 1031.

Tajima, T. 1989 "Computational Plasma Physics" (Addison-Wesley, Redwood City).

Zirin, H. 1988 "Astrophysics of the Sun" (Cambridge U.P., Cambridge).

Figure Captions

Figure 1(a). Solution of the simplified particle equations of motion, given by equations (2.5), for the case of constant Alfvén velocity.

Figure 1(b). Same as Figure 1(a), but for an Alfvén velocity which increases with height.

Figure 2. Initial density distribution for electrons. The average number of electrons per zone is approximately 10 (indicated on the figure by n_0). All other particles followed the same density distribution law.

Figure 3. Photon spectrum computed from the final electron energy spectrum, assuming bremsstrahlung to be the dominant energy-conversion mechanism.

Figure 4. Final ($t = 800\omega_{pe}$) electron energy spectrum.

Figure 5. Phase-space plot for electrons of normalized longitudinal momentum versus grid position.

Figure 6. Final proton energy spectrum.

Figure 7. Like Figure 5, but for protons.

Figure 8. Final energy spectrum for ^{4}He. Note the highly non-thermal region from approximately 1 MeV to 10 MeV.

Figure 9. Phase-space plot for ^{4}He.

Figure 10. Normalized transverse momentum versus normalized longitudinal momentum for ^{4}He. There is substantial preferential longitudinal acceleration for these ions.

Figure 11. Like Figure 8, but for ^{3}He. Again there is a strong deviation from a thermal distribution in the high-energy region.

Figure 12. Like Figure 9, but for ^{3}He.

Figure 13. Like Figure 10, but for ^{3}He. The preferential longitudinal acceleration is again evident.

Figure 14. Total z-component of magnetic field, at the final time $t = 800\omega_{pe}$. The leading edge of the fast magnetosonic wave can be seen at approximately $x = 820$.

Postal Addresses

Katherine A. Holcomb CGD Division NCAR P.O. Box 3000 Boulder, CO 80307

Toshiki Tajima Institute for Fusion Studies Department of Physics University of Texas Austin, TX 78712

Baruch Meerson Center for Plasma Physics Racah Institute of Physics Hebrew University Jerusalem, Israel

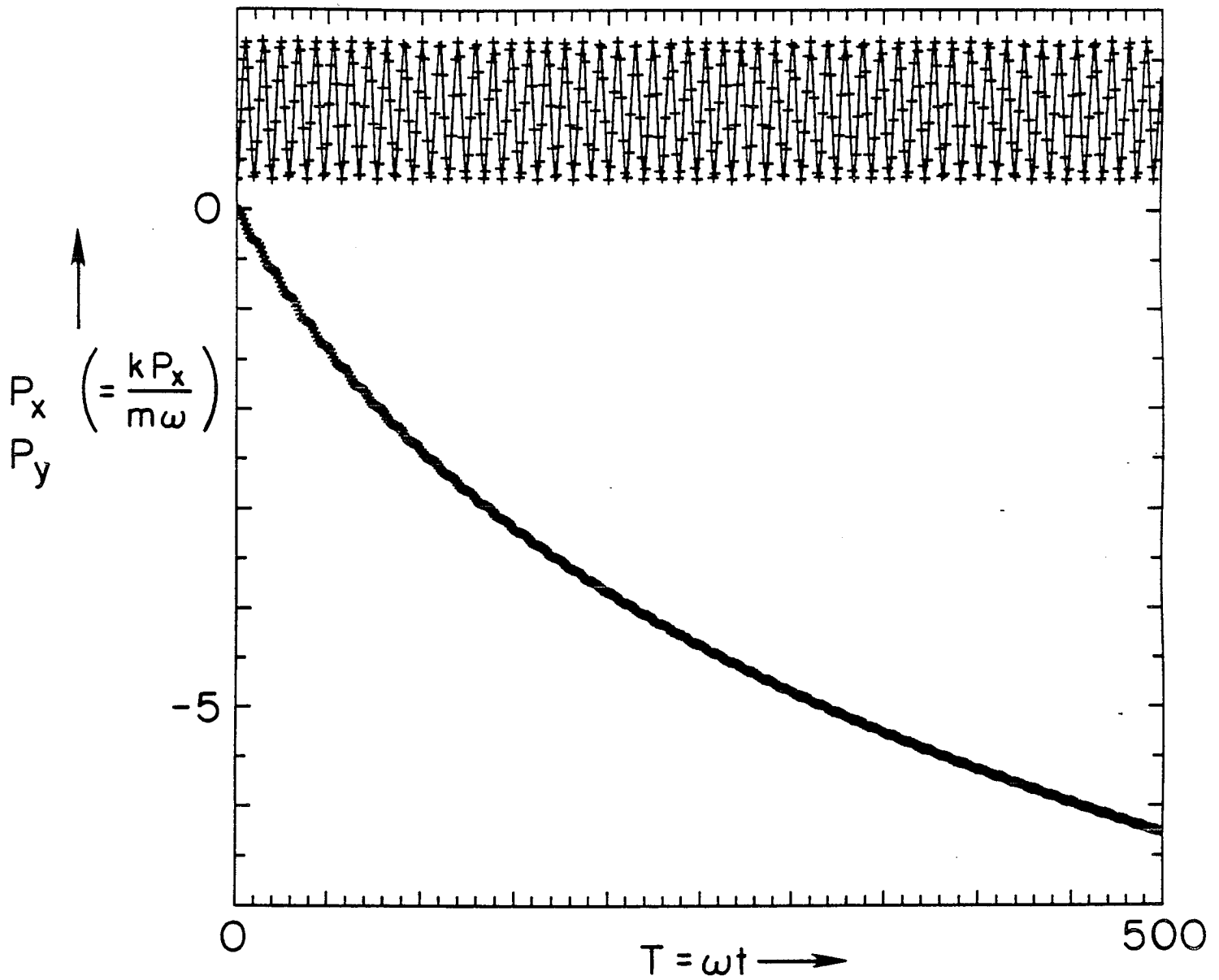

Fig. 1(a)

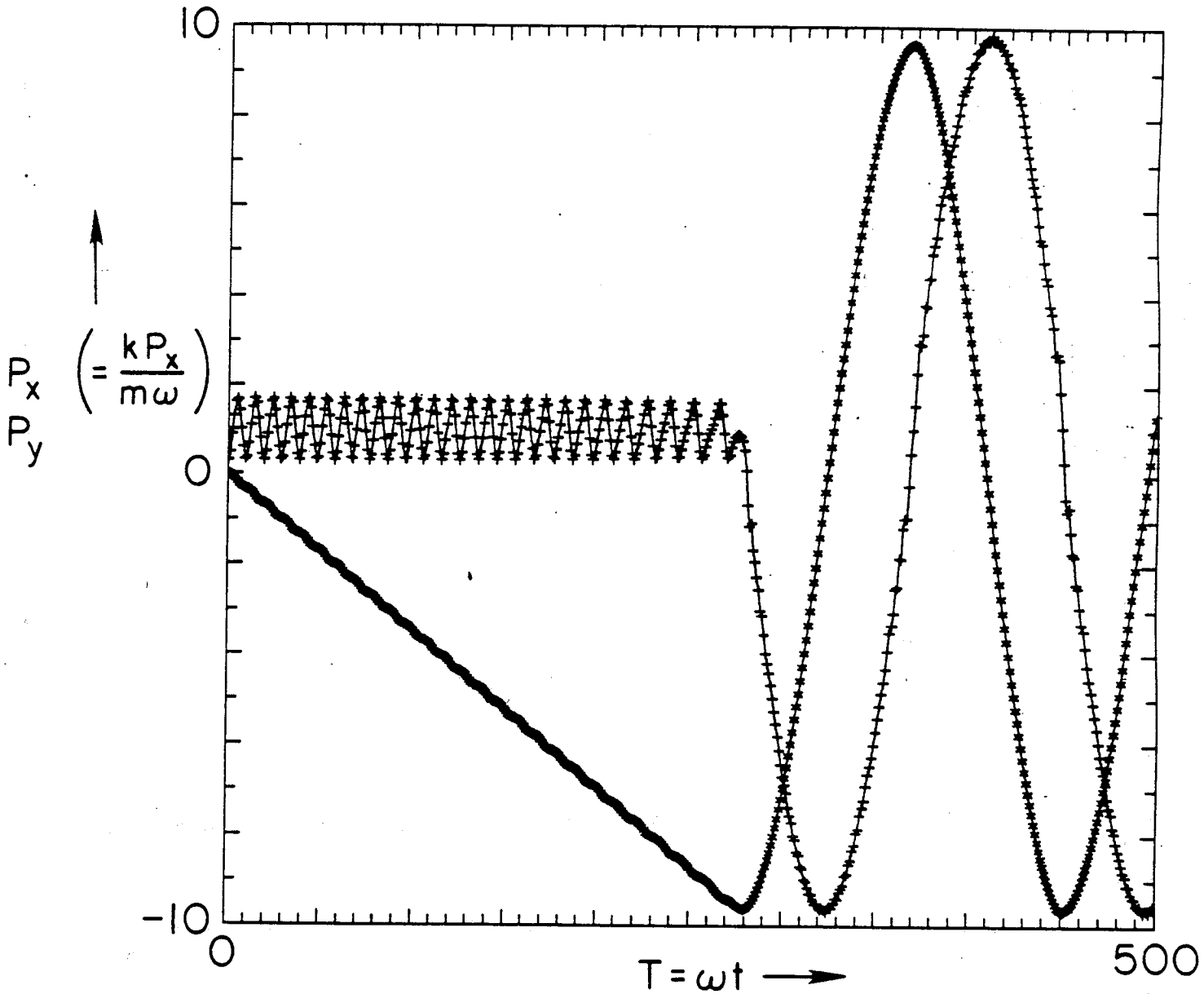

Fig. 1(b)

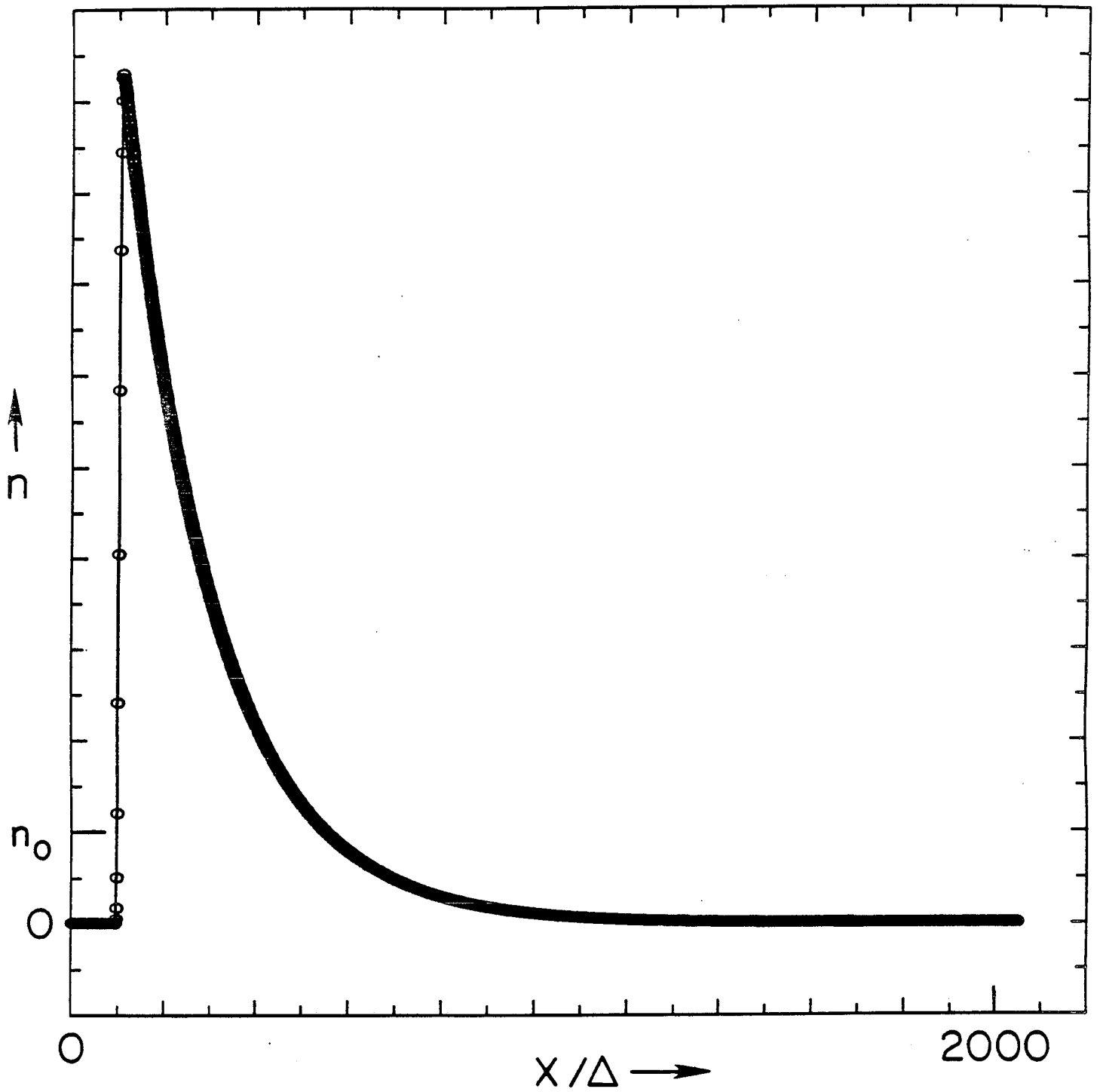

Fig. 2

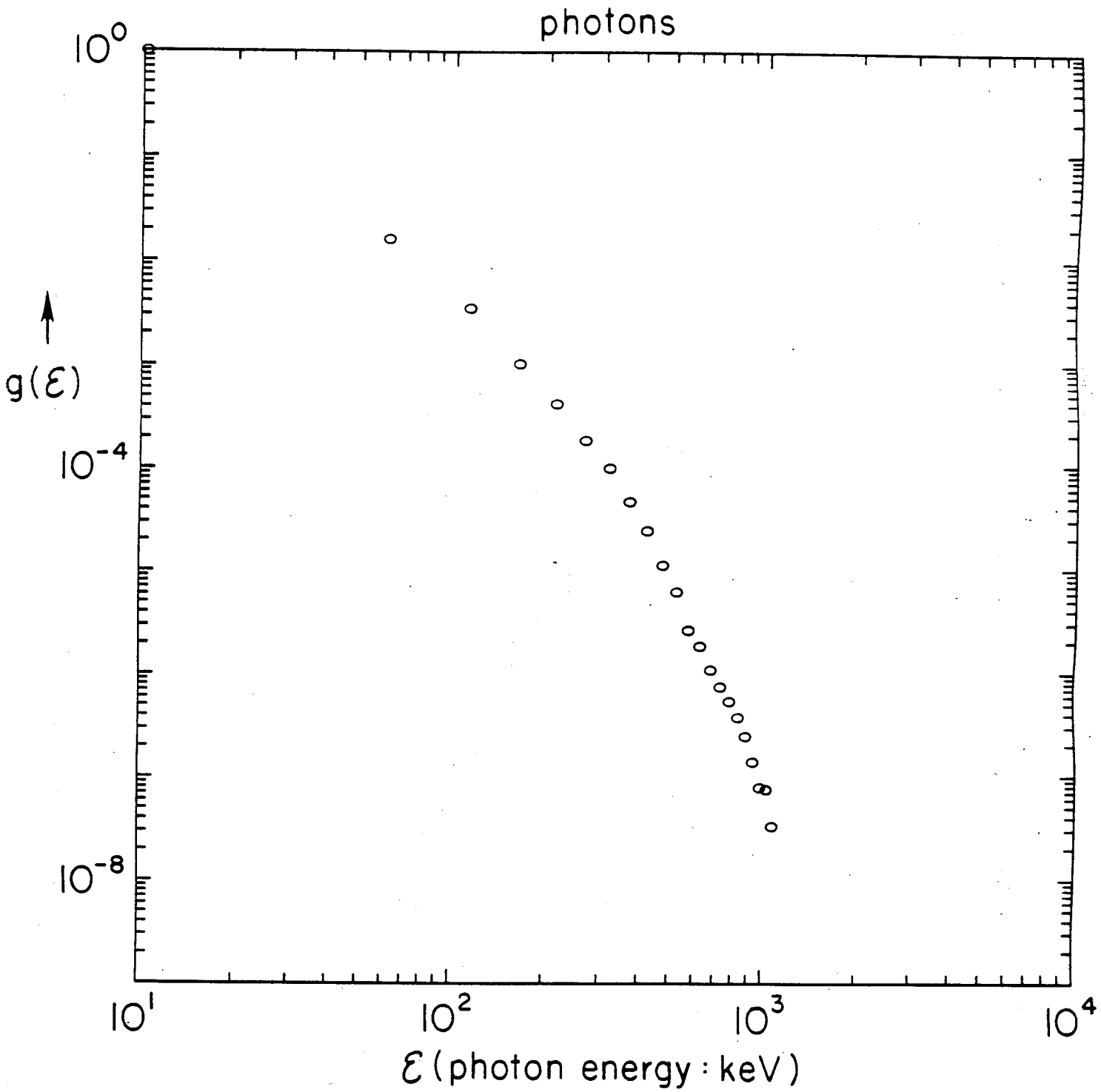

Fig. 3

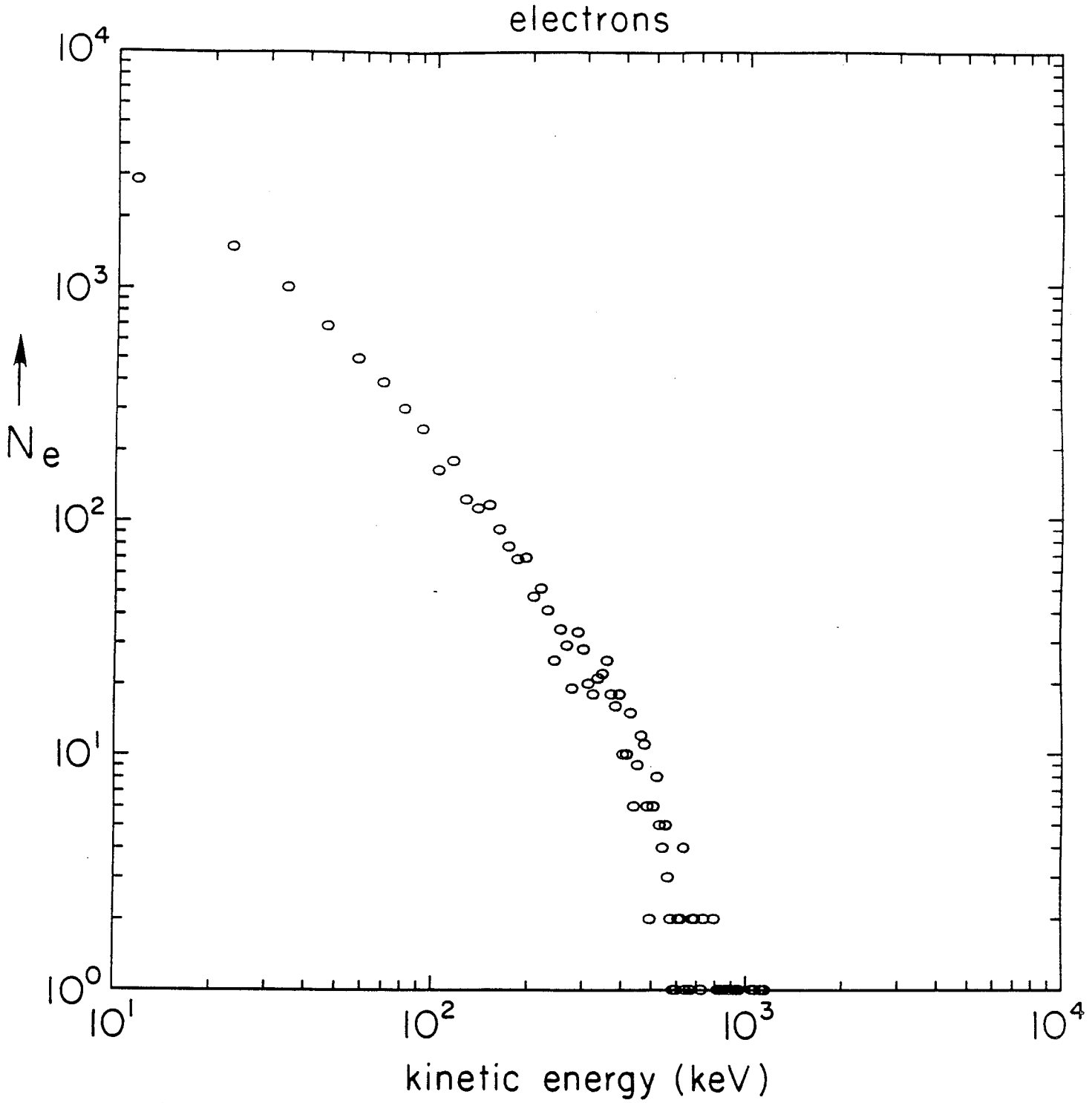
electrons
10^4
10^3
10^2
10^1
10^0
N_e
10^1
10^2
10^3
10^4
kinetic energy (keV)

Fig. 4

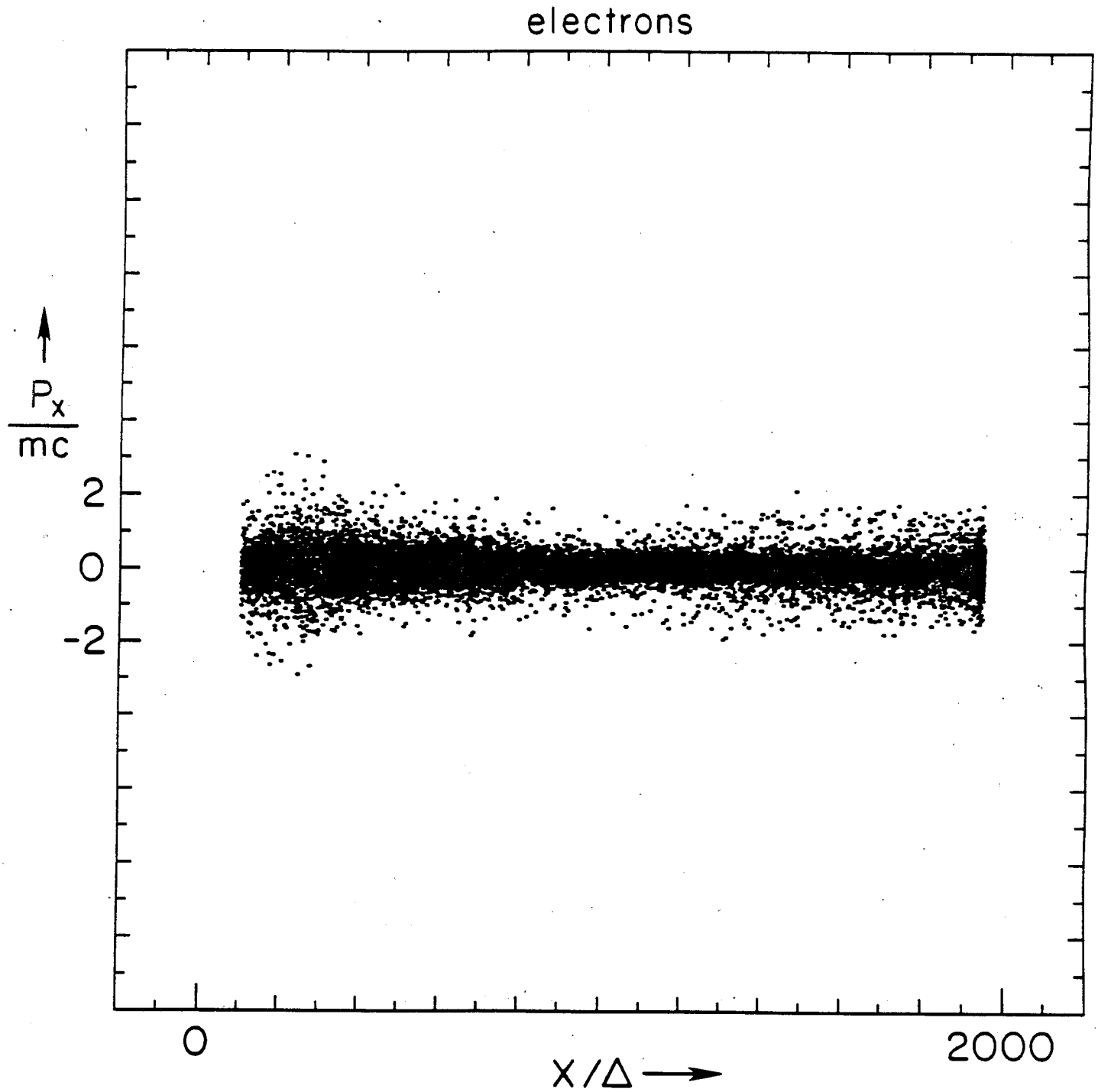

Fig. 5

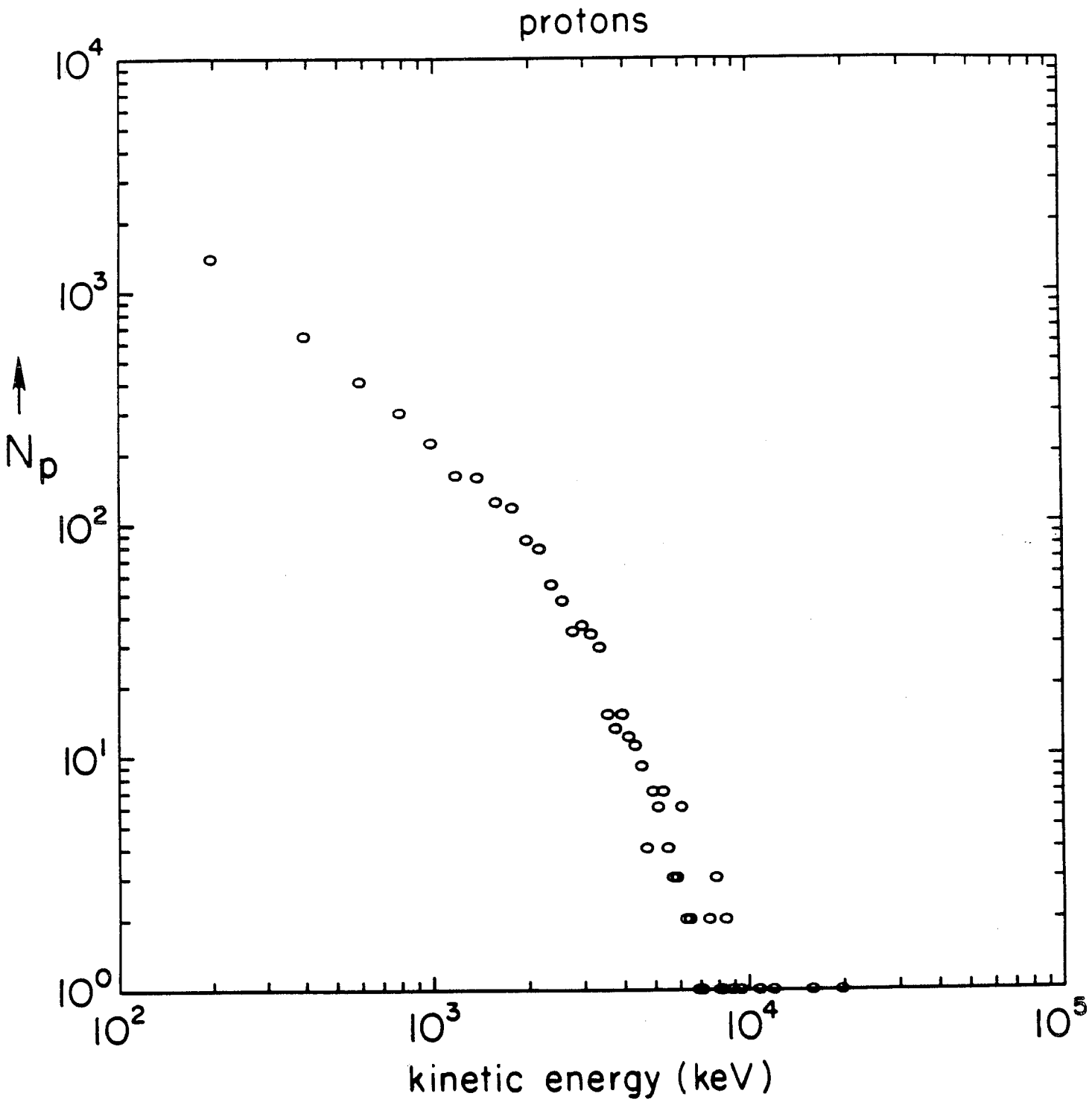
protons
10^4
10^3
10^2
10^1
10^0
N_p
10^2
10^3
10^4
10^5
kinetic energy (keV)

Fig. 6

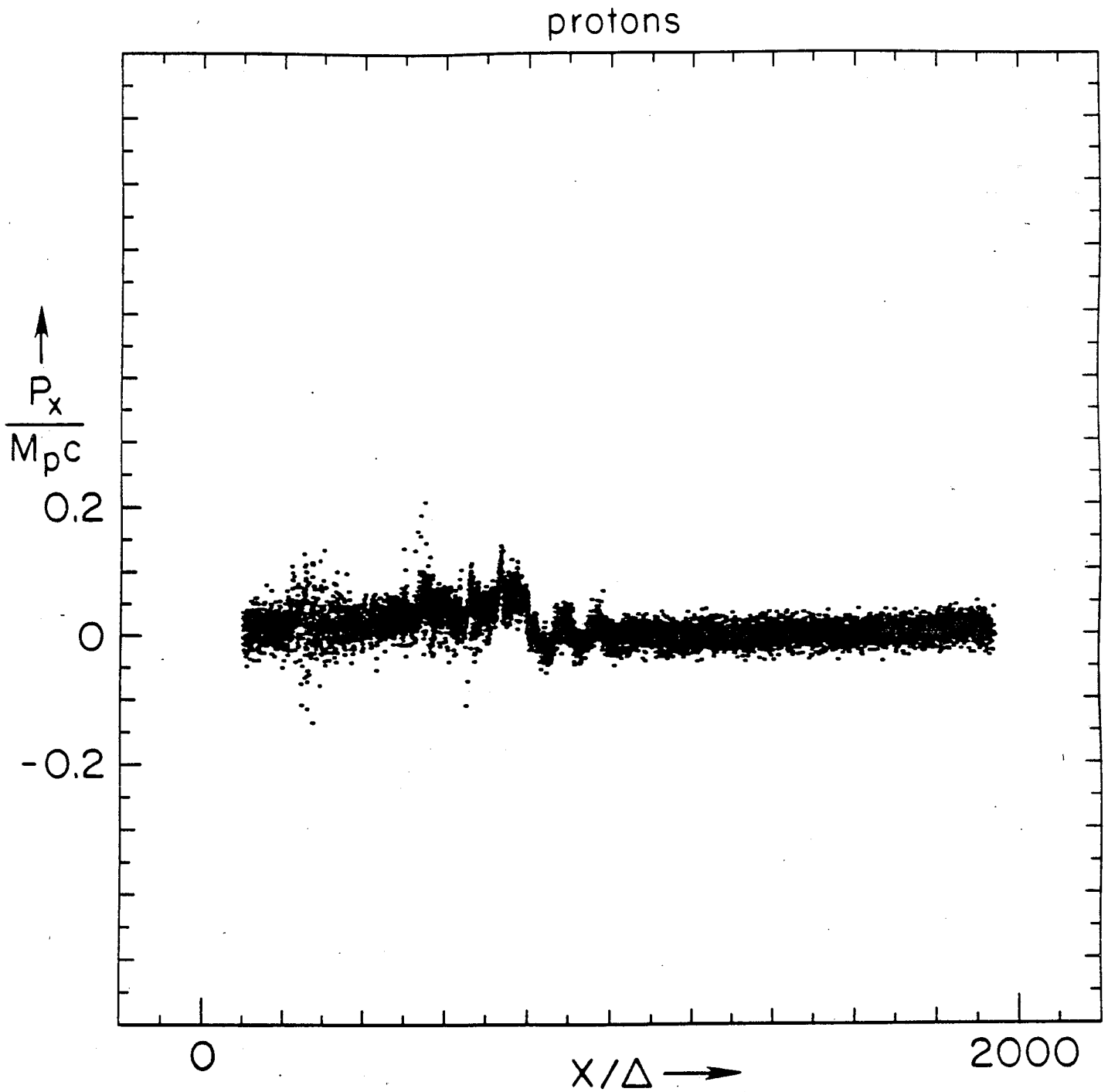

Fig. 7

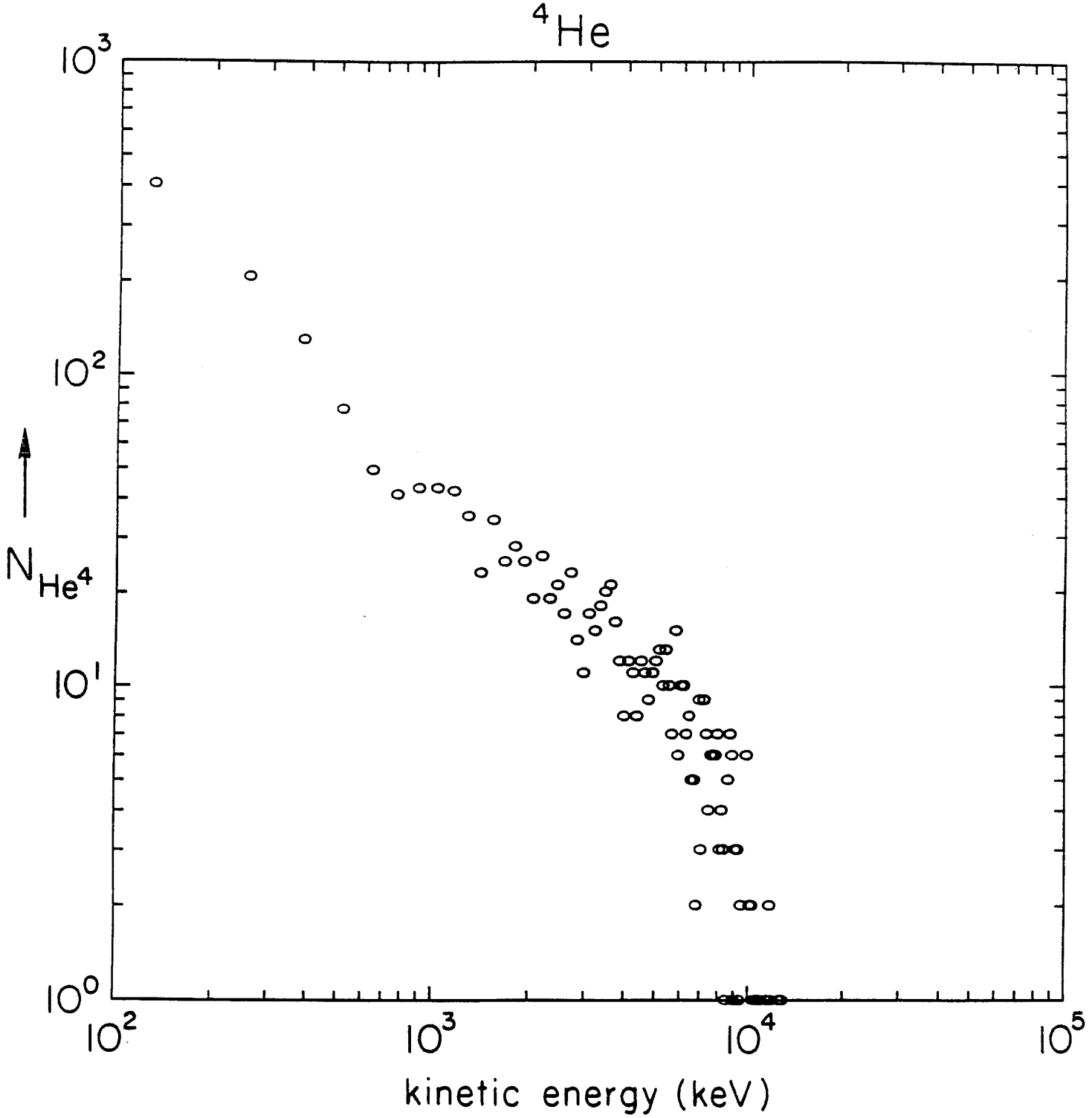

Fig. 8

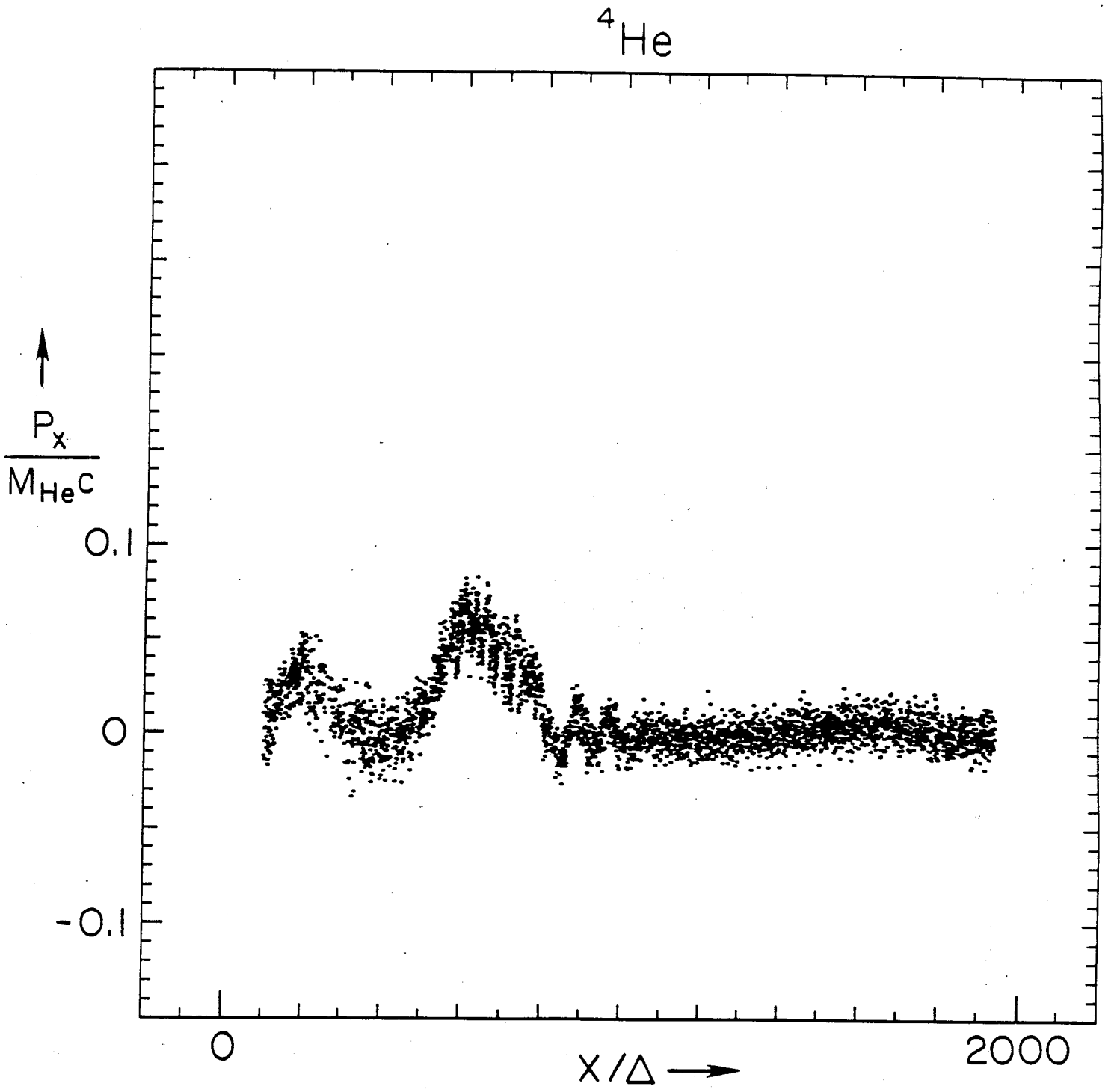

Fig. 9

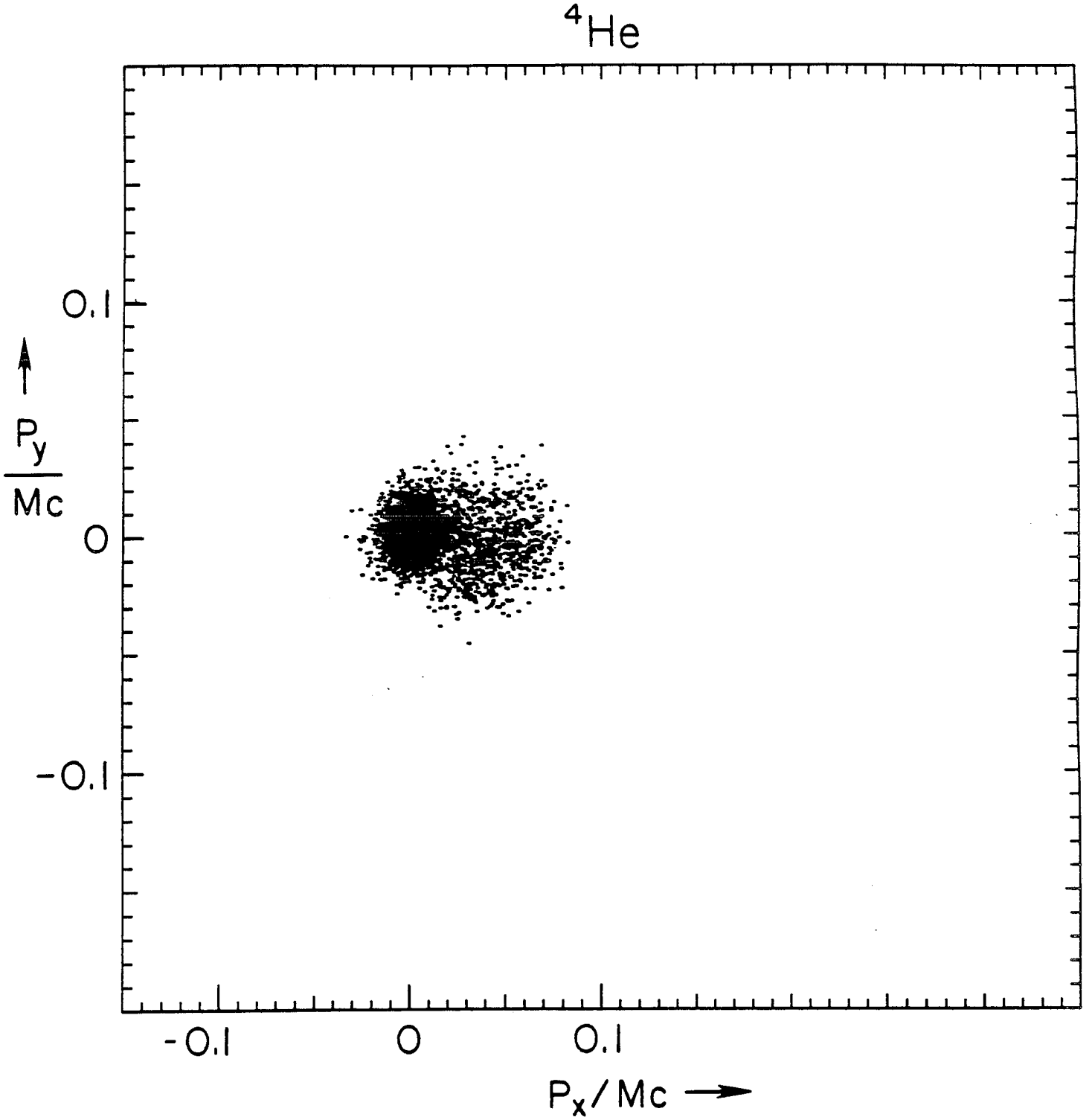

Fig. 10

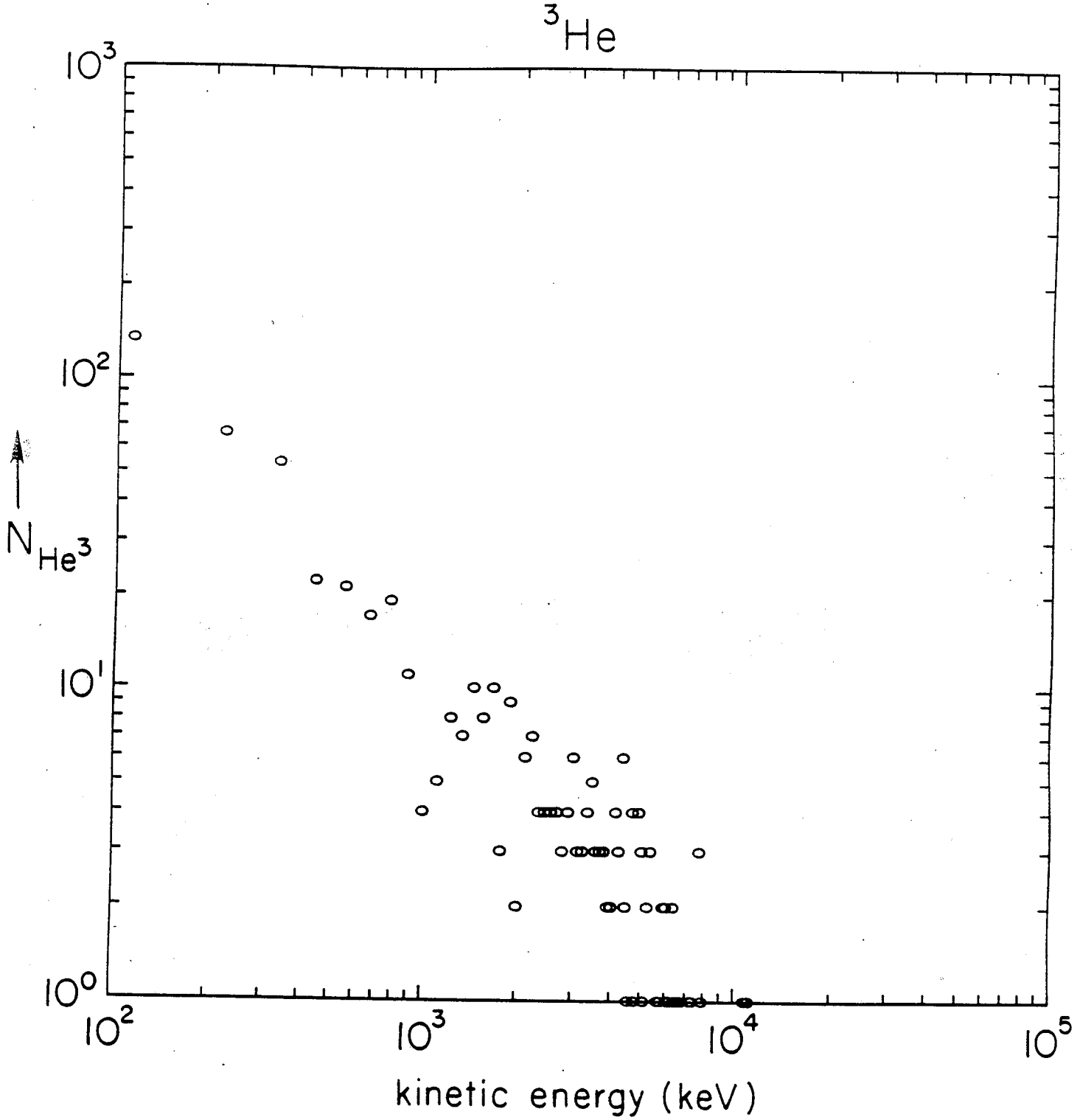

Fig. 11

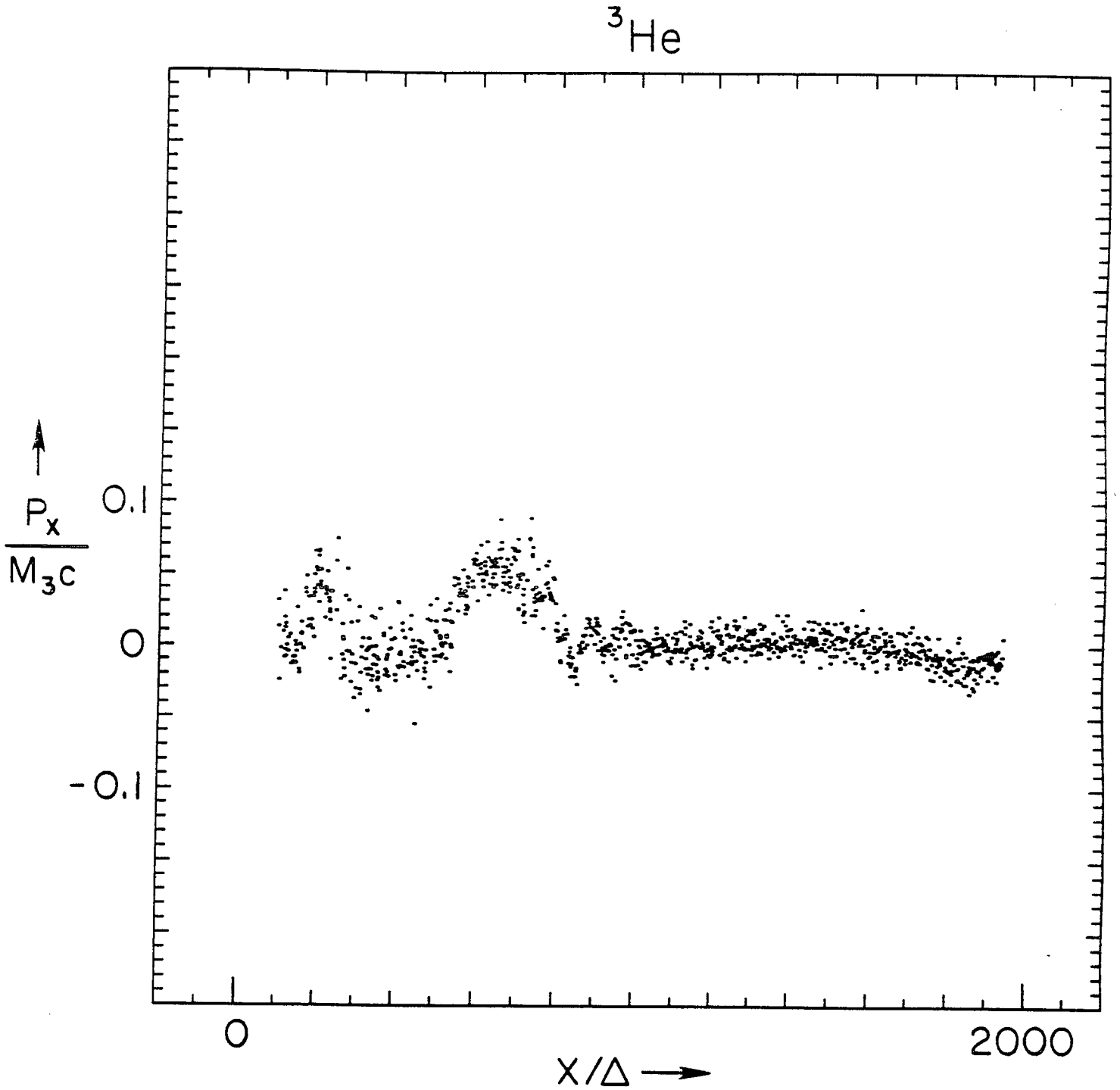

Fig. 12

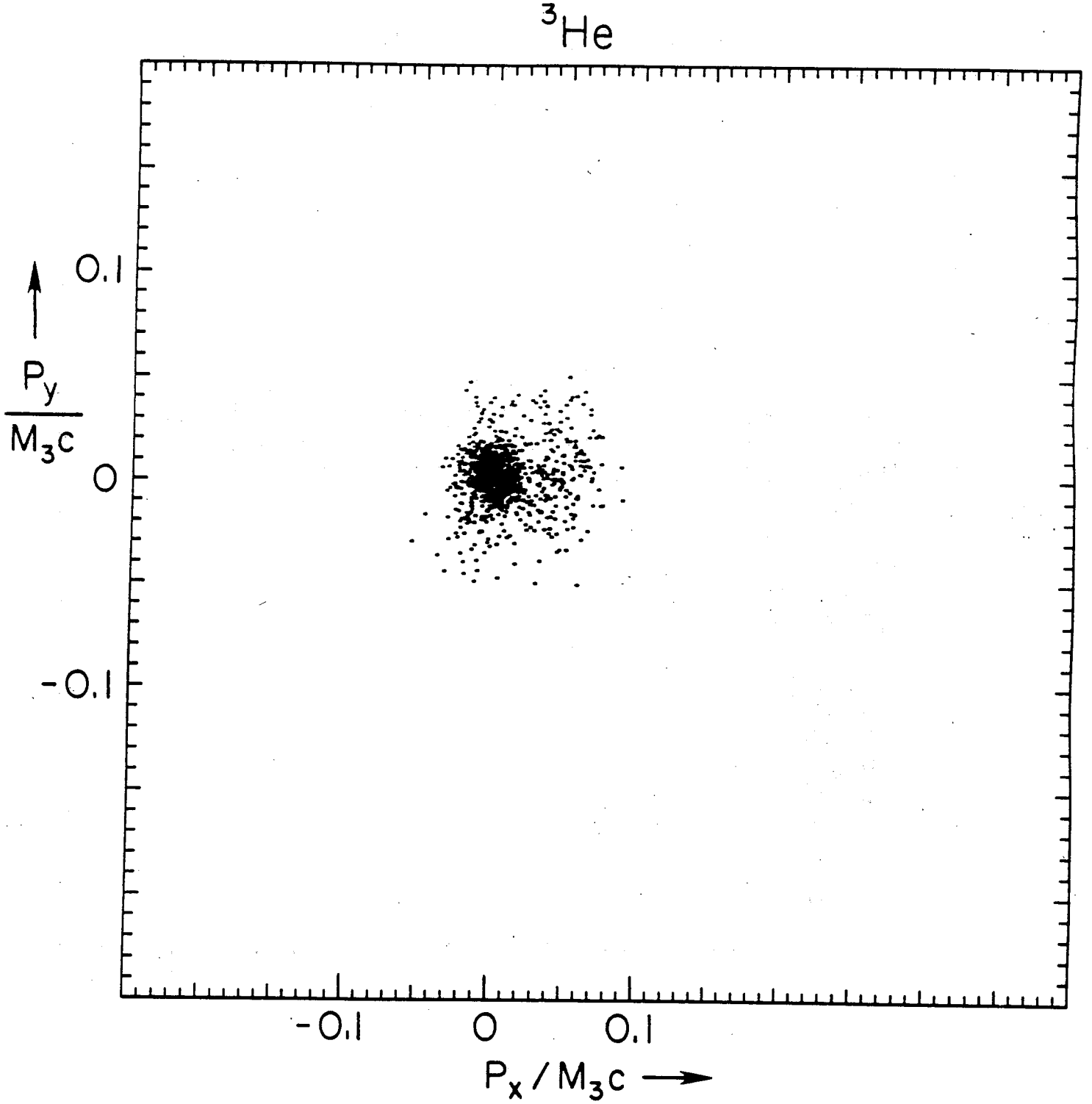

Fig. 13

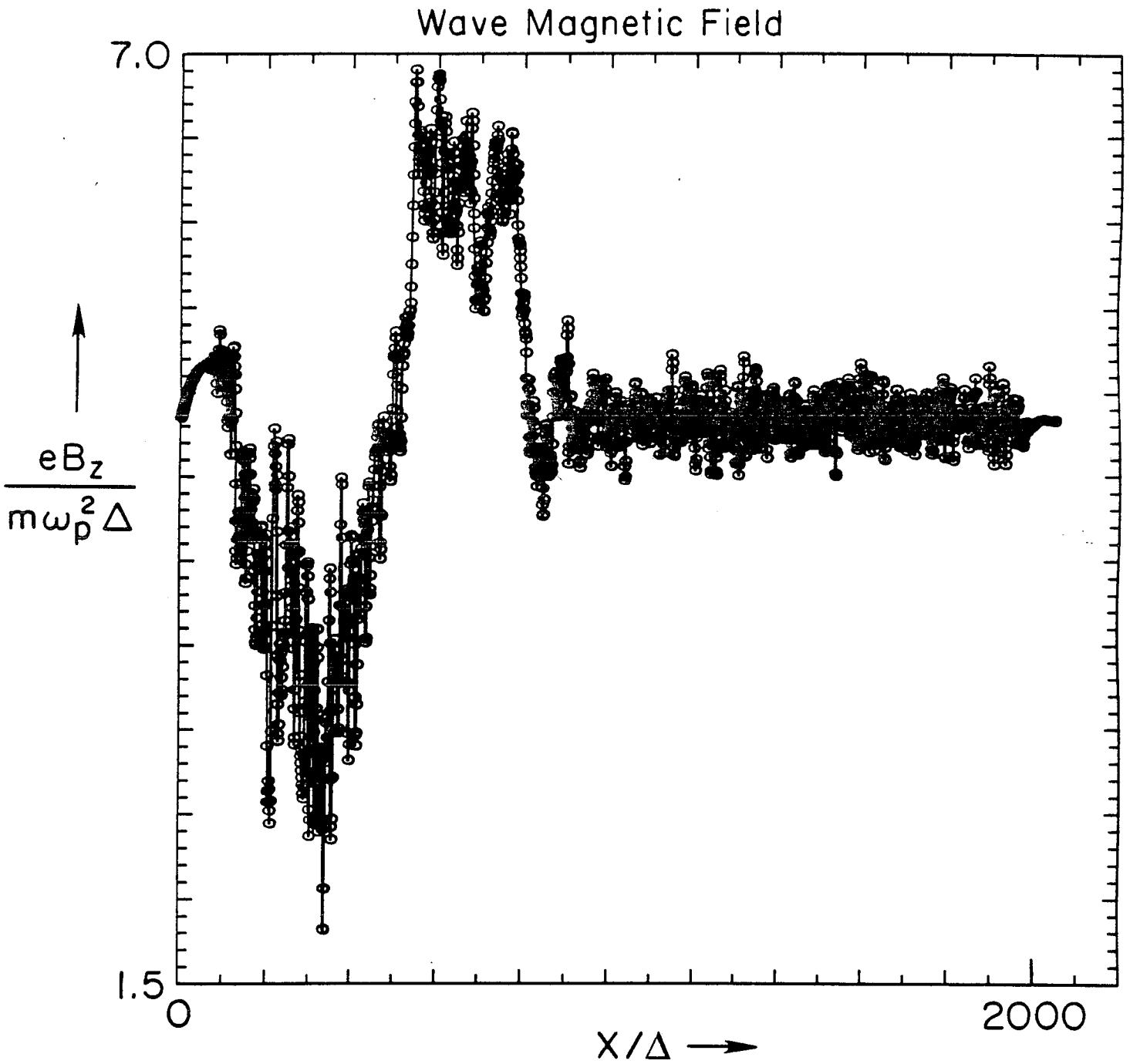

Fig. 14